Optics Development for the SPEAR Mission

Kwangsun Ryu[a], Kaori Nishikida[b], Jerry Edelstein[b], Kwangil Seon[c], Insoo Yuk[c], Kyungwook Min[a], Wonyoung Han[c], Eric Korpela[b], Ray Chung[b], and Ken McKee[b]

[a] SaTReC, KAIST, 373-1 Kusong-dong, Yusong-gu, Taejon, Korea
[b] Space Sciences Lab., U.C. Berkeley, California 94720-7450, U.S.A.
[c]KAO, 61-1 Whaam-dong, Yusung-gu, Taejeon, Korea

ABSTRACT

We describe the development of optics for the SPEAR space-mission to map the far ultraviolet (900–1750 Å) sky. The SPEAR spectrometers contain unusual reflective optics to optimize sensitivity to diffuse emission. We describe the manufacture, test and performance of the collecting mirrors: Pyrex parabolic cylinders with a 90 degree off-axis angle. We also describe the development of the diffraction gratings: ellipses of rotation that are holographically-ruled with constant spacing and blazed with ion-beam ablation.

Keywords: far ultraviolet, spectrometer, parabolic cylinder, grating

1. INTRODUCTION

Space observation in the far ultraviolet region provide important information about various physical processes occurring in the interstellar media. SPEAR (Spectroscopy of Plasma Evolution from Astrophysical Radiation) is a diffuse far ultraviolet(long wavelength band: 900–1150Å, short wavelength band: 1335–1750Å) imaging spectrometer, designed to trace the balance and flow of energy through Galactic plasma.

To obtain a large grasp factor within the small payload size allowed within a micro satellite, a parabolic cylinder mirror is used. Optical parameters are determined through rigorous ray tracing and tolerance analysis.

Manufacturing and testing of the off-axis parabolic cylinder mirror was a critical issue in development of the SPEAR system. We have explored interferometric testing of the off-axis parabolic mirror figure. We describe testing experiments and result of an off-axis cylinder mirror using a CGH null as a reference surface and line spread function measurement at the position of the slit using knife edge scanning method is introduced.

We also describe the development of the diffraction gratings: ellipses of rotation that are holographically-ruled with constant spacing and blazed with ion-beam ablation.

2. SPEAR OPTICAL SYSTEM AND TOLERANCE ANALYSIS

As depicted in figure 1, each SPEAR optical channel uses a parabolic cylinder mirror to focus a collimated beam along one axis to a slit. The elliptical grating focuses along the other axis while dispersing light to spectrum. The optical system is able to obtain angular image in along-slit-direction and to scan the sky across along-slit-direction. At the focal plane, an MCP is employed as a detector. A shutter assembly in front of the slit adjust the effective area to observe bright sources such as aurora and geo-coronal emissions.

Based on the conceptual design, we optimized the optical parameters to satisfy our scientific requirements. The optical performance of SPEAR was considered geometrically and radiometrically. The geometric performance was analyzed by investigating the point spread function and resolution. The calculation was done both using commercial ray-trace code and by solving equations of wavefront aberration. The results are compared and found to be essentially the same.

Through an optimizing process, we established the specifications of the optical system and estimated the tolerance limit of manufacturing. We estimated that angular resolution varies within $5' \sim 10'$ while spectral resolution varies within $2 \sim 5$Å, according to the wavelength and field angle. The resulting specifications are listed in table 1. The off-axis parabolic cylinder mirror has a focal length of 125 mm and f/# of 2.2.

Further author information: (Send correspondence to Kwangsun Ryu)
Kwangsun Ryu: E-mail: ksryu@satrec.kaist.ac.kr

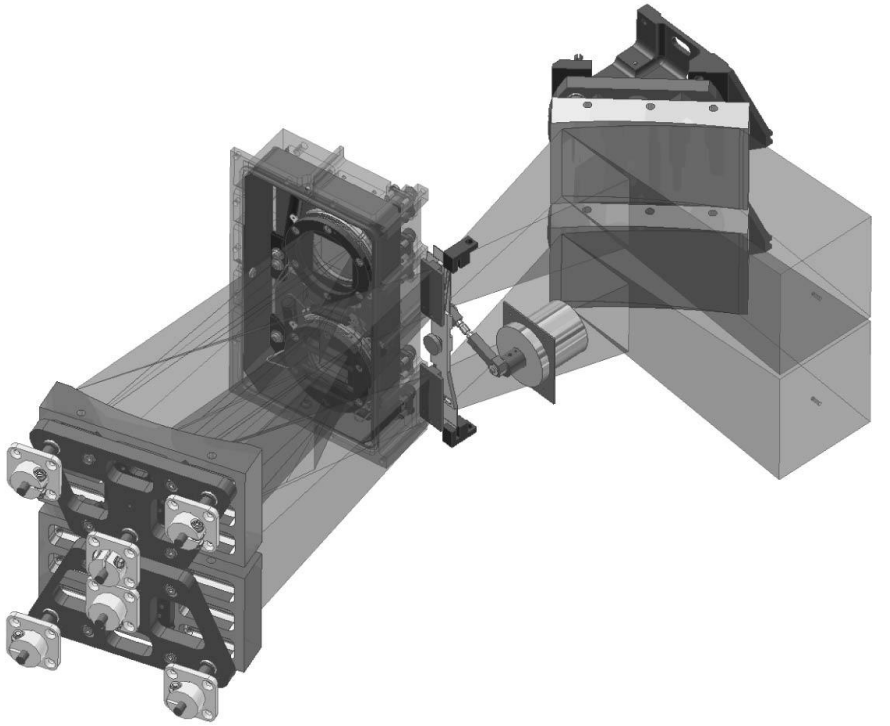

Figure 1. Schematic diagram which represents operation principle of SPEAR optics

Radiometric performance was characterized by effective grasp which relates the intensity of emission sources and detected signal. The value was derived by multiplying geometric area, reflectivity of the optical components, quantum efficiency of the MCP, and solid angle where the detector sees. Based on the effective grasp value of $\sim 1.0\times10^{-4}\mathrm{cm}^2\mathrm{sr}$, we have estimated the detection possibility of the diffuse emission and compared with the previous observations. It is revealed that one-year survey can discriminate how the galactic emission sources are distributed.

After the optimization and radiometric analysis of the SPEAR optics, tolerance analysis is followed to design the mounting and adjustment scheme. From the scientific requirement that C IV and O VI line should be distinguished from geo-coronal emission within the limited exposure time, we have derived the criteria of the optical performance as listed in table 2. Based on the criteria, the allowable range of motion, tilt and rotation of the optical components and that of optical parameters themselves were investigated along with their coupling and independence.

Once more than two optical parameters are found to be coupled, one of the parameters is fixed and then the other parameter is studied to see if it can compensate the errors. In case when an optical performance is coupled with a component parameter and a geometric parameter, then we loosen the specification of the optical component and let the geometric parameter be adjustable to compensate the error. As an example, both the radius of curvature of the ellipsoidal grating and the position of the grating in optical axis are sensitive to spectral resolution. We loosen the specification of the grating to extent where the compensation by the geometric adjustment can allow.

3. MANUFACTURING AND TEST OF OFF-AXIS PARABOLIC MIRROR

Among the optical parts, the off-axis parabolic mirror is an unusual and difficult item to manufacture. At the first stage, the risk was that we don't have the testing method, to say nothing of manufacturing itself. So we studied cylinder mirror test methods. There are several methods to interferometrically test cylindrical optics. A simple way is to use a plane reflection at the focal line. In this case, the light does not return along the same path. Consequently, the fringe pattern contains information only about errors that are symmetrical about the center plane. The interpretation is less than straightforward.

Table 1. FIMS optical specifications

Instrument Parameters	Short Wavelength Band	Long Wavelength Band
Band Pass	900–1150 Å	1335–1750 Å
Field of View	[a] 4°×5′	8°×5′
Mirror Figure	Off-axis Parabolic Cylinder	Off-axis Parabolic Cylinder
Mirror Focal Length	125±2 mm (F/2.2)	125±2 mm (F/2.2)
Off-axis angle θ	90±1.5°	90±1.5°
Mirror Substrate Size	50 × 93.35 × 17.5 mm	50 × 93.35 × 17.5 mm
Mirror Figure Quality	0.8 λ(P-V) per cm 633 nm	0.8 λ(P-V) per cm 633 nm
Surface Roughness	25 Å	25 Å
Slit Height	2.75 cm	2.75 cm
Slit Width	150 μm	150 μm
Grating Figure	Ellipse of Rotation	Ellipse of Rotation
Ellipse Axis A (spectral)	180.0 mm	180.0 mm
Ellipse Axis C	242.6 mm	242.6 mm
Toroid Radius ρ	326.97 mm	326.97 mm
Ruling Constant G	2250 lines/mm	3000 lines/mm
Diffraction Order	Second Inside	First Inside
Detector Size	2.5×2.5 cm^2	2.5×2.5 cm^2
Detector Pixels	512×512	512×512
Mirror Coating	B_4C	MgF_2
Grating Coating	B_4C	MgF_2
Photocathode	KBr	CsI + Grid
Fixed Filter	MgF_2	CaF_2
Effective Grasp	0.6×10^{-4} cm^{2}sr	1.25×10^{-4} cm^{2}sr

[a] 4°×5′ for background observation

An alternative plan is to use an optical fiber as a reference surface(Geary[2] , 1995) instead of using a mirror at the focal line. We performed a preliminary experiment on a standard on-axis cylinder mirror using an Al-coated optical fiber, but found the setup so sensitive to the position and tilt of the optical fiber that we failed to obtain a stable interference pattern. We found it difficult to obtain the tension required to keep the optical fiber straight.

Recently, testing aspheric surfaces(Arnold et al.[3] , 1995) with commercially available CGH's has become common. We used a CGH cylinder null 'H45F1.5C'(Diffraction International[4]) to experiment with testing a standard on-axis cylindrical mirror. The CGH diffracts a collimated beam from a Feazeu type interferometer to a f/1.5 cylindrical beam with quality of $\sim \lambda/10$.

Table 2. Performance criteria of FIMS optical system to get scientific goals

Performance	Criteria	Comments
Spectral Resolution	<1.8Å at 1035Å	[a]For O_{VI} line detection
	<3.0Å at all short wavelength band	
Spatial Resolution	$< 10'$ at all wavelength and all θ	To get same spatial resolution as ϕ
Bore Sight Error in [b]θ	$< \pm 1°$	Half of FOV overlap in θ
Bore Sight Error in [c]ϕ	$< \pm 2.5'$	Half of FOV overlap in ϕ
Wavelength Shift	< 30Å	$\sim 1/10$ shift in a band

[a]Seon et al.,[1] (2000)
[b]θ : field angle along slit direction
[c]ϕ : off-axis angle along scan direction

3.1. Manufacturing Process of Parabolic Cylinder Mirror

The mirror profile can be described by simple one-dimensional quadratic function, $y = ax^2$, where the coefficient a is determined by the focal length. Since we use a 90° off-axis configuration, the coordinate system is rotated by 45°. Then the profile is described as the following equation.

$$y = \frac{2x + \sqrt{2}/a - \sqrt{(2x + \sqrt{2}/a)^2 - 4(x^2 - \sqrt{2}x/a)}}{2} \tag{1}$$

Because the parabolic cylinder is not symmetric about the optical axis, it is impossible to shape the substrate using turning-based machines such as diamond turning method. Instead, we used a computer controlled CNC machine in the process of substrate shaping and grinding. The precision of the grinding process is under 4μm. The profile error was measured by a contact-type 3 dimensional measurement system.

After measuring the profile at 10 by 10 points throughout the substrate, grinding by hand was iterated until the error decreases to under $\sim 2\mu$m. For errors less than 2 μm, stylus profile measurement and interferometric testing substitute for contact-type measurement to further guide the polishing process. The polishing was iterated based on the measurement to meet the profile specification of $\sim \lambda$/cm. When the profile come close to the specification, the micro roughness was also monitored using micro interferometer to reduce the scattering in the wave length band.

3.2. Test of Cylinder Mirror Using CGH

Our CGH null diffracts a collimated laser beam to generate a cylindrical reference beam of f/1.5. Because of the nature of diffraction patterns, the CGH generates beams of other orders. The CGH is designed to use order +1 or -1. One is corresponding to converging beam and the other corresponding to diverging beam. A schematic diagram which represents the method of using the CGH in testing cylinder surface is shown in figure 2(Ryu et al.[5] , 2000). A slit at the CGH focal line blocks the diverging beam from the CGH.

The test is done in two steps to measure the off-axis parabolic cylinder. First, CGH is dedicated to measure the profile error of an on-axis cylinder mirror. Then we get the interference fringe for the off-axis mirror using the measured on-axis mirror as a reference. The reason that CGH is not directly used in measuring the parabolic cylinder mirror is related with degrees of freedom in the test setup and efficiency of the CGH. Since the efficiency of the CGH is less than 10% and the cylinder mirror is not coated, the interferometer cannot make fringe pattern clear enough to measure. If we use on-axis cylinder mirror as a reference, the number of axis to be adjusted in fine step ($\sim 1\mu$m) reduces from 5 to 3.

Figure 2 shows the test setup and fringe pattern for the on-axis cylinder mirror. As can be seen in figure 2(a), the on-axis cylinder mirror is measured with a CGH proving that it can be used as a reference. After aligning the mirror to minimize the fringe number as figure 2 (a), the profile error of the cylinder mirror is measured using phase shift technique. Over the entire cylinder surface, the profile error is less than $\lambda/5$ which is enough to be used as a reference since our specification for the parabolic cylinder mirror is $\sim \lambda$/cm.

Figure 3 shows the methods and results of interferometric measurement for SPEAR parabolic cylinder mirror. In figure 3(a), the measurement technique called 'cat's eye configuration' which uses a flat mirror at the focal plane is presented. As shown in figure 3(b), the fringe pattern is formed symmetrically with respect to the cylindrical center. This is because the light reflected from the reference flat mirror travel to the conjugate path instead of the same path along which the light travel before the reflection.

The experimental setup to measure the parabolic cylinder mirror using a reference cylinder mirror is represented in figure 3(c). It is not plausible to align two optical component at once as represented in the figure. After aligning the parabolic cylinder mirror with respect to pre-aligned flat mirror as figure 3(a) so that the parabolic cylinder mirror form a line focus 90° off axis from the collimated beam, we can get fringe pattern in figure 3(d) by adjusting the reference cylinder mirror. Once the number of fringes in the entire parabolic surface reduces to several, phase shift technique can yields the divergence of the parabolic surface from the ideal surface.

In figure 4, the profile error measured by stylus profilometer and by interferometer is shown. In the entire region, the measurement error is less than 0.2μm while the error diverges up to 0.5μm in the edge where the slope is high. This difference is considered as a result of tendency that the error is cumulated around the region where the slope is relatively high in case of interferometer test. Measurement result from the 'cat's eye configuration' is also plotted with

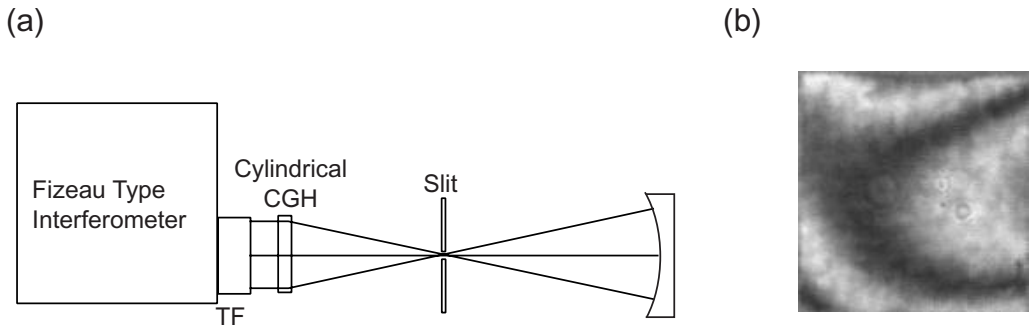

Figure 2. (a) Schematic diagram of interferometric measurement on on-axis cylinder mirror and (b) the fringe pattern of the cylinder mirror used as a reference mirror.

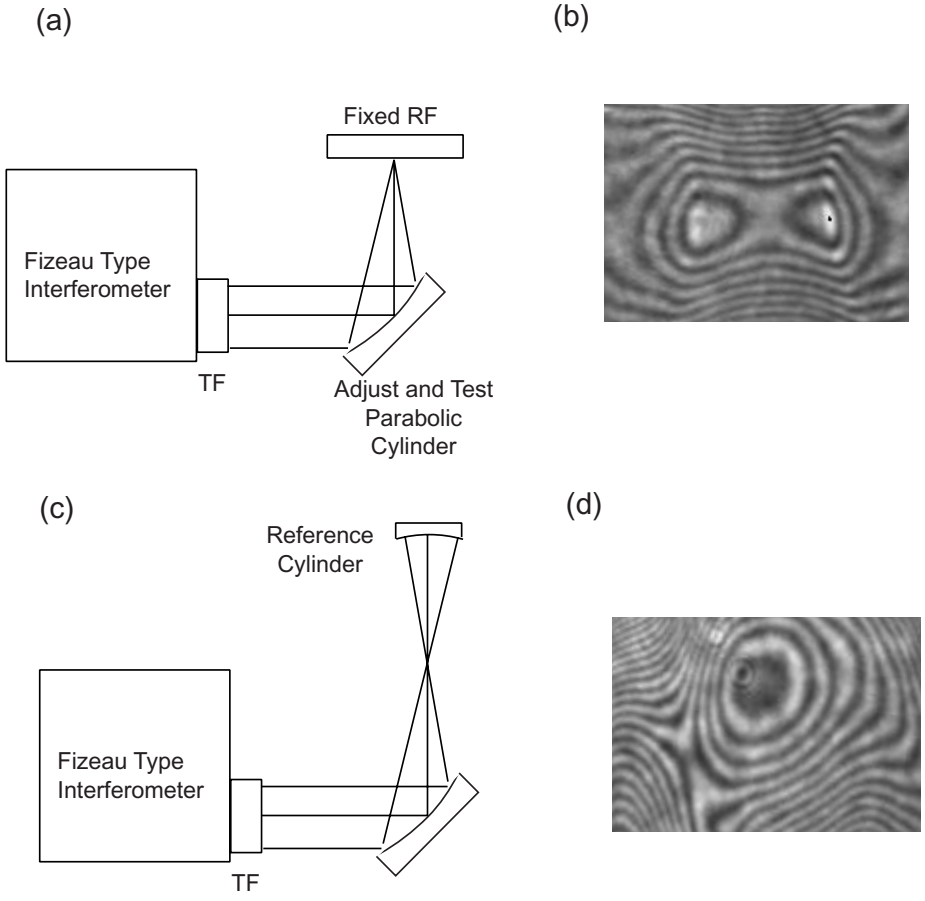

Figure 3. Schematic diagram and fringe pattern of the interferometric test on the off-axis parabolic cylinder mirror. (a) test using flat mirror as a reference, (b)fringe pattern obtained from the experiment (a), (c) test using cylinder mirror as a reference, and (d)fringe pattern obtained from the experiment (c)

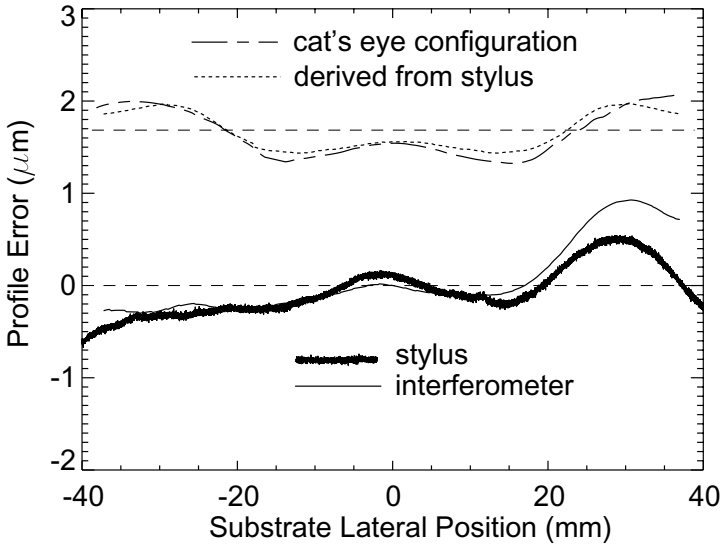

Figure 4. Profile error measured by stylus profilometer and interferometer. Plotted above is the profile error measured by the 'cat's eye configuration' with the even component derived from the profilometer measurement.

the even component value derived from profilometer measurement 2μm shifted from the reference. The overall results show that the interferometric measurement can complement the profilometer method in that the interferometer can measure the error in the entire surface at once while the profilometer can provide the precise value in the restricted path along which the profile is scanned.

3.3. Line Spread Function and Micro-Roughness as Final Check

The optical performance of the parabolic cylinder mirror is finally represented by line spread function at the slit position. Knife edge scanning method is used in the measurement for the SPEAR parabolic cylinder mirror. A collimated beam incident on the parabolic surface is focused on the focal plane 45° tilted from the optical axis. A knife edge mounted on a finely controllable X-Y linear stage is located around the focal line. Then the parabolic cylinder mirror and the knife edge is adjusted for the line focus and aligned with the knife edge to minimize the line profile using a microscope located behind the knife edge.

Once the best focus is found and aligned with the knife edge, the integrated line spread function is measured by moving the knife edge in 1μm step. A PM tube is used as a photometric sensor in the experiment. The line spread function measured by knife edge scanning is represented by solid curve in figure 5. As can be seen in the figure most of the energy (95%) is falling within 100 μm which quite less that the slit width (150μm).

The LSF can also be derived from the profile measurement using a first order approximation and is also plotted with a broken line. The derivation of the LSF from the profile measurement is simply described as the following equation.

$$\Delta Y_{\text{focal plane}} = f \times \frac{\Delta y}{\Delta x} \tag{2}$$

where $\Delta Y_{\text{focal plane}}$ means lateral position in the focal plane, f focal length, and $\Delta y/\Delta x$ the slope of the profile deviation from the ideal parabolic surface respectively. The result shows that the approach is coincident with the measurement and the performance is directly related with the slope error of the mirror surface.

In addition to the profile error, micro-roughness is also an important parameter which determines the optical performance since the value is directly related with scattering. According to Geary (1993), the total integrated

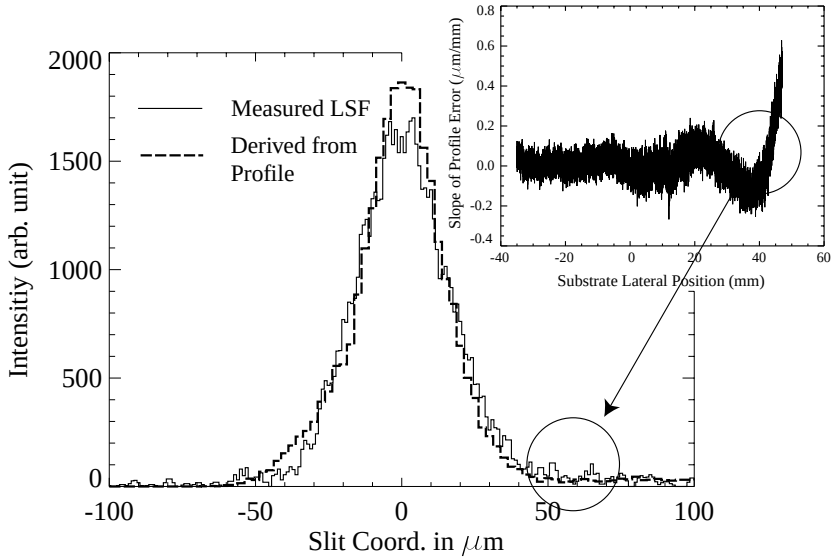

Figure 5. Measured line spread function is co-plotted with estimation using profile error. Large deviation of profile is thought to be responsible for the tail in line spread function.

scatter which represents the ratio of scattered energy to the reflected (specular and diffuse) energy is related with micro-roughness R_q (RMS: Root Mean Square) as

$$R_q = (\frac{\lambda}{4\pi \cos\theta})\sqrt{TIS}, \tag{3}$$

where θ is the angle from the surface normal and is corresponding to $\sim 45^\circ$ for the SPEAR mirror.

The effect on the SPEAR optical performance by scattering can be analyzed by considering the stray light outside the field of view. We have considered the effect of geo-corona and stray light from the nearby stars which emits a large amount of UV flux and derived the minimum requirement of the micro-roughness of 25Å. We have attempted pitch polishing using a copper pad to follow the asymmetric and anamorphic surface. We obtained 10Å rms surface roughness over the surface. The surface roughness was measured using a Veeco NT2000 micro interferometer which has a 0.1 nm resolution. According to the equation (3), the energy loss due to scattering is less than 2% in the SPEAR spectral range.

4. MANUFACTURING OF ELLIPSOIDAL GRATING

Zeiss Optics is manufacturing the flight diffraction gratings. The grating uses a blazed profile produced by chemically etching a holographically-formed pattern into glass. Other parameters of the gratings are listed in Table 1. We measured the grating efficiency of a sample grating provided by Zeiss. A plane coating witness sample was also provided by Zeiss. The sample grating is spherical with a radius of curvature of 250 mm, and has a groove density of 2250 lines/mm. The grating is continuously ion-blazed to optimize efficiency over the range of working illumination angles over the short wavelength band (900–1150Å).

4.1. Relative Efficiency

In order to obtain the relative efficiency of the grating, we first measured the reflectivity of the gold coating on the grating from the witness sample. Measurements were made with oxygen and hydrogen emission lines at 878Å, 1027Å, 1152Å, and 1216Å. The sample was illuminated with a UV beam through a monochrometer and the reflected light was detected with a MCP. Background measurements were taken at "off-line" wavelengths close to each emission line profile in the spectral space. Background-subtracted reflected count rate was divided by background-subtracted

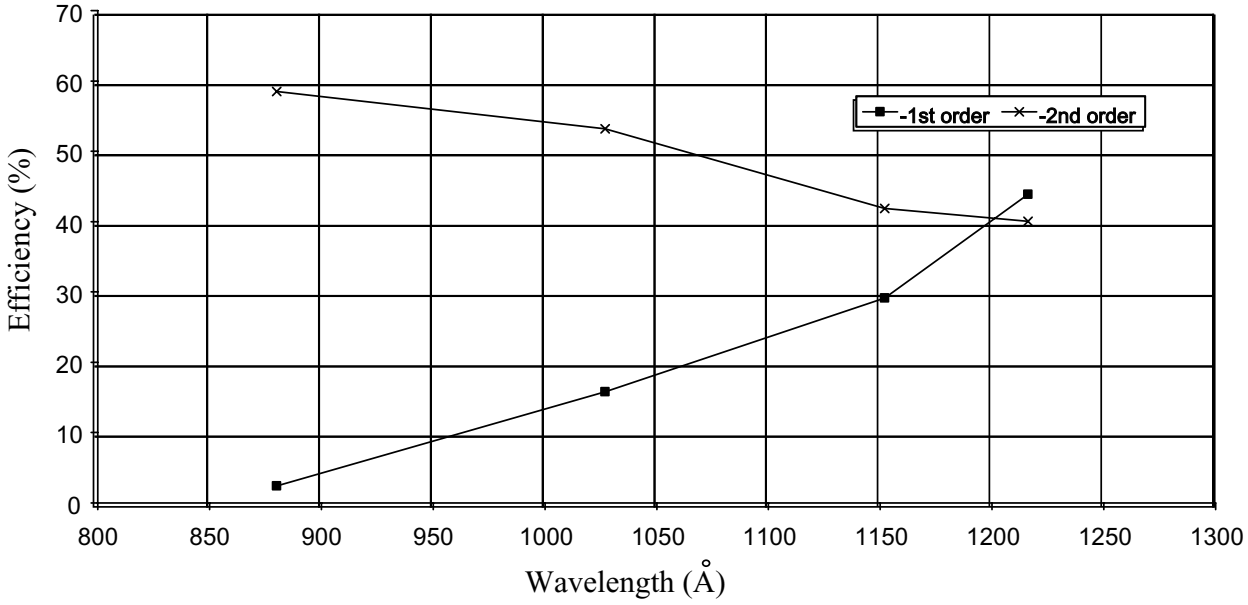

Figure 6. The measured relative efficiency of the sample grating at inside 1st order and 2nd order

through beam count rate to obtain the surface reflectivity. The reflectivity varied from 15% at 878Å to 18% at 1216Å.

We measured the relative efficiency of the sample grating at inside 1st order and 2nd order. The inside 2nd order is used in the flight configuration. We illuminated the center of the grating with a UV beam (small compared to the total grating surface area) through a monochrometer. The incident angle of the beam was 21.9°, same as the flight configuration at the center of the grating. The measurements were taken in a similar manner to the surface reflectivity measurements. The absolute efficiency thus obtained was divided by the surface reflectivity to yield the relative efficiency. We show the relative efficiency in Figure 6. The plot shows that the blaze has markedly improved the performance compared to a non-blazed sinusoidal profile grating.

We also measured the efficiency as a function of position (horizontal) on the grating surface at 878Å and 1027Å at the inside 2nd order. The results are shown in Figures 7 and 8. The variation of relative efficiency over the surface is due to the varying grove profile to optimize efficiency at 1027Å.

4.2. Lyman-alpha Scattering

Lyman-alpha emission scattered by the grating is a major source of noise in the short wavelength band. Therefore we measured the scatter from Ly-alpha at the center of the short wavelength band. The measurement was taken in a similar manner to the surface reflectivity measurements. The detector covered approximately half the wavelength band, centered at 1025Å. Assuming the scattering profile is uniform across the band, we measure a ratio of scattered light to incident flux to be 7.2×10^{-6}/arcmin with ~10% measurement error.

5. SUMMARY

We have introduced the design procedure and specifications for the SPEAR optics. Manufacturing and testing of an off-axis parabolic cylinder mirror for SPEAR is a critical issue in development of the system. We have studied methods of testing cylindrical optics and found a valuable method of using a CGH null which generates a cylindrical wavefront. Using the test method, we have manufactured the parabolic cylinder mirror that satisfies the optical specification derived from the scientific requirements.

Finally, we described the test result of the grating efficiency and scattering for the sample diffraction grating being manufactured by Zeiss Optics.

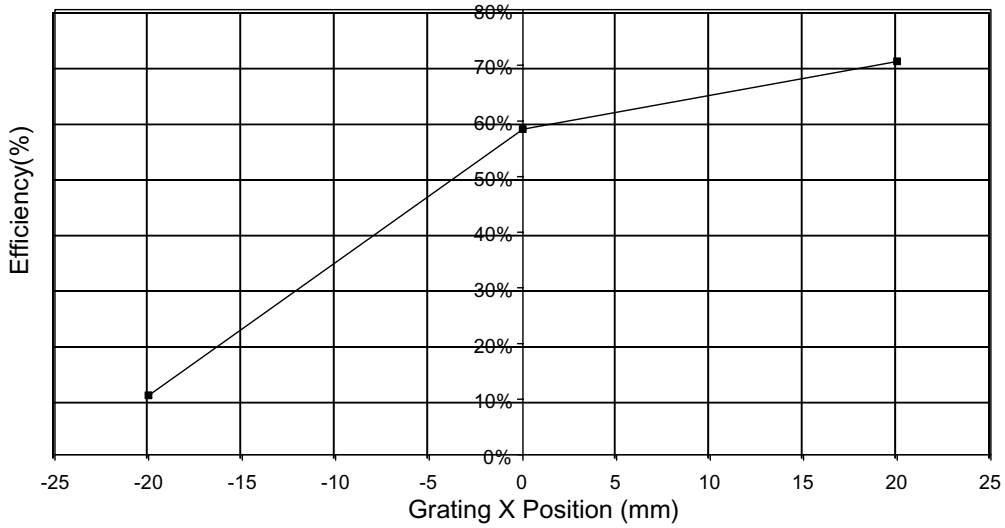

Figure 7. The measured diffraction efficiency as a function of horizontal position on the grating surface at 878Å.

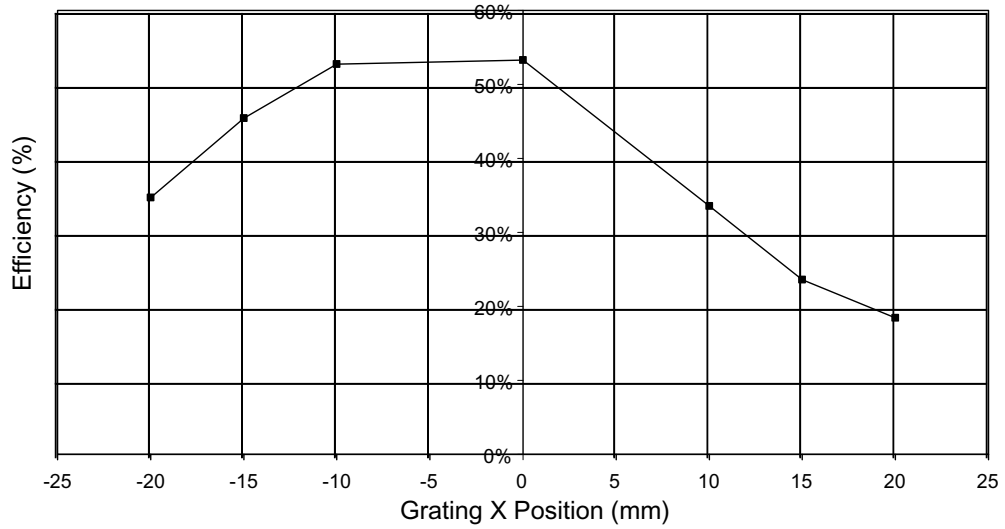

Figure 8. The measured diffraction efficiency as a function of horizontal position on the grating surface at 1027Å.

ACKNOWLEDGMENTS

This work has been conducted in support of KAISTSAT-4 program funded by Korean Ministry of Science and Technology and by NASA Space Astrophysics and Research Grant NAG-5355.

REFERENCES

1. K. I. Seon, K. S. Ryu, I. S. Yuk, J. H. Park, U. W. Nam, W. Han, J. H. Seon, K. W. Min, J. Edelstein, and E. J. Korpela, "O vi emission line detection limit of far ultraviolet imaging spectrograph," *J. Astro. Space Sci.* **17**, pp. 77–86, 2000.
2. J. M. Geary, "An overview of cylindrical optics tesing using a fiber optic reference," in *Optical Manufacturing and Tesing*, V. J. Doherty and H. P. Stahl, eds., *Proc. SPIE* **2536**, pp. 68–74, 1995.
3. S. M. Arnold, L. C. Maxey, J. E. Rogers, and R. C. Yoder, "Figure metrology of deep general aspherics using a conventional interferometer wiht cgh null," in *Optical Manufacturing and Tesing*, V. J. Doherty and H. P. Stahl, eds., *Proc. SPIE* **2536**, pp. 106–116, 1995.
4. Diffraction International, 11345 Hwy. 7, #421, Minneapolis, Minnesota 55305.
5. K. S. Ryu, J. Edelstein, J. B. Song, Y. W. Lee, K. I. S. J. S. Chae, I. S. Yuk, E. J. Korpela, U. W. Nam, W. Han, and K. W. Min, "Testing method of off-axis parabolic cylinder mirror for fims," in *Advanced Optical Manufacturing and Testing Technology 2000*, *Proc. SPIE* **4231**, pp. 312–319, 2000.